CNRS
Centre National de la Recherche Scientifique

INFN
Istituto Nazionale di Fisica Nucleare

Acoustic characterization of Advanced Virgo buildings

VIR-0673A-18

Mikel Falxa, Donatella Fiorucci, Irene Fiori, Federico Paoletti, Jan Harms, Matteo Barsuglia

Issue: 1

Date: October 5, 2018

VIRGO * A joint CNRS-INFN Project
Via E. Amaldi, I-56021 S. Stefano a Macerata - Cascina (Pisa)

Contents

1 Introduction

The detection of low frequency gravity signals faces some major issues. In particular, ground based Gravitational Wave (GW) detectors will be affected by various contributions of Newtonian Noise (NN). Below 1 Hz, one of the main sources of this noise are the atmospheric infrasound waves [1] .

This work aims to analyze the impact of the acoustic normal modes of the buildings containing the GW detectors on the infrasound NN level. In this respect, several acoustic measurements were performed inside the North End Building (NEB) at the Advanced Virgo (AdV) site to allow the study of the distribution of such modes and to highlight their effects.

In the present document, we briefly introduce what the Newtonian Noise is and present its different possible origins. Then, after some recalls of acoustics, we will discuss the results of our measurements.

Figure 1: AdV site, the NEB is on the top right corner of this image, at the end of the interferometer's arm.

2 Newtonian noise (NN)

A local perturbation of density leads to a perturbation of the gravity field. As these variations are tiny, newtonian gravity is enough to describe them. For a variation $\delta\rho(\vec{r},t)$ of the density, we have a variation $\delta\Phi(\vec{r_0},t)$ of the gravitational potential at point $\vec{r_0}$ as :

$$\delta\Phi(\vec{r_0},t) = -G\int dV \frac{\delta\rho(\vec{r},t)}{|\vec{r}-\vec{r_0}|} \tag{2.1}$$

with G the gravitational constant and dV the element of volume.

On Earth, we observe different sources of fluctuations of the gravity field associated to different mechanisms of density variation [3]. In the case of GW laser interferometers, these gravity field perturbations induce motions in the test masses generating a displacement noise which degrades the observations of the signals of interest.

2.1 Seismic Newtonian noise

The seismic "Newtonian" noise must not be mistaken with the seismic noise. The latter is due to the continuous vibration of the Earth with an amplitude of a few microns. This movement has many origins : the anthropogenic activity (local traffic, trains, ...), the local phenomenons like wind and also the background activity of micro-earthquakes [4]. The seismic "Newtonian" noise corresponds to the perturbation of the gravity field induced by the variation of density of Earth's crust caused by a seismic wave passing through.

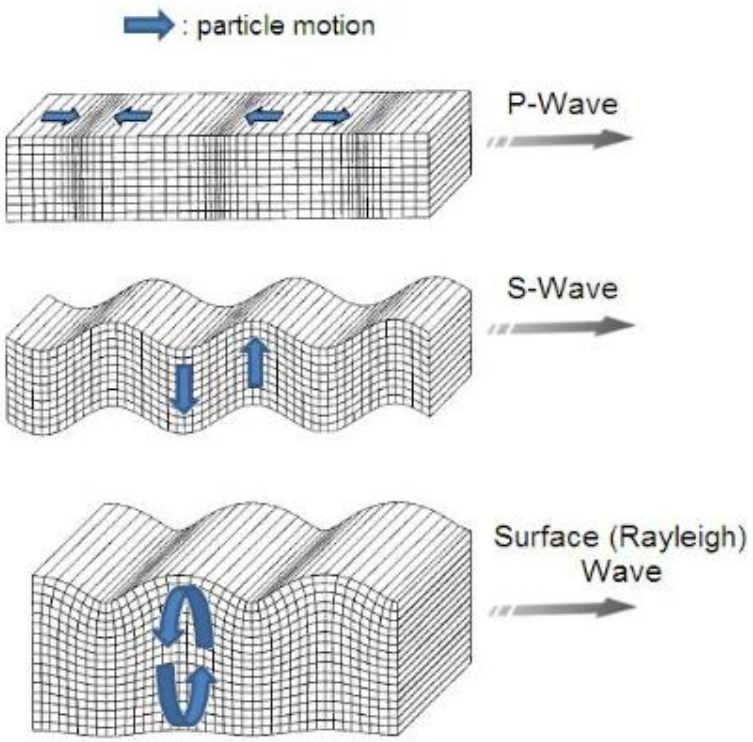

Figure 2: Different types of seismic waves.

2.2 Atmospheric Newtonian noise

2.2.1 Infrasound

The atmospheric Newtonian noise is linked to the changes in atmospheric density. Sound waves are one of the sources of density fluctuations in the atmosphere. They correspond to the propagation of a little pressure perturbation around the mean pressure value p_0. At low frequency, we can relate these pressure changes to the density changes using the given formula :

$$\gamma \frac{\delta\rho(\vec{r},t)}{\rho_0} = \frac{\delta p(\vec{r},t)}{p_0} \tag{2.2}$$

where $\gamma \simeq 1.4$ is the heat capacity ratio.

Using equation 2.1, we obtain an expression for the variation of the gravity field with respect to the pressure fluctuations. Therefore, acoustic measurements of the sound field are required to estimate the corresponding Newtonian Noise.

2.2.2 Temperature fluctuations

Local perturbation of the gravity field can also come from atmospheric temperature fluctuations since they lead to density perturbations. Considering small variations of temperature and the law of ideal gas at constant pressure, we get :

$$\delta\rho(\vec{r},t) = -\frac{\rho_0}{T_0}\delta T(\vec{r},t) \tag{2.3}$$

where ρ_0 and T_0 are the mean atmospheric density and temperature.

As with the infrasounds, we can write a direct relation between the variation of the gravitational potential and temperature. The noise coming from these fluctuations does not affect current GW laser interferometers. However, it can become relevant at low frequencies. In this respect, we underline that below a few tens of mHz it is necessary to develop new atmospheric models which take into account the influence of the Earth surface temperature on the atmopheric temperature fluctuations.

2.2.3 Shockwaves

Atmospheric shockwaves can generate brutal changes in pressure which lead to transient signals in the detector rather than participating to the background noise.

Figure 3 illustrates the variation of the gravitational acceleration felt when a shockwave hits the detector for different velocities of the source (α being the speed of sound). This type of noise is usually easy to veto using environmental sensors around the detector test masses.

2.2.4 Turbulent phenomenon

The sound produced by turbulent flows is also a source of Newtonian noise and is treated with Lighthill theory. The calculation is done using some approximations given the complex behavior of turbulence (uniform temperature, stationary, homogeneous and isotropic velocity field, inferior to sound speed). Here we only want to mention that this noise does not affect current laser interferometer sensitivities, but it can be significant for the

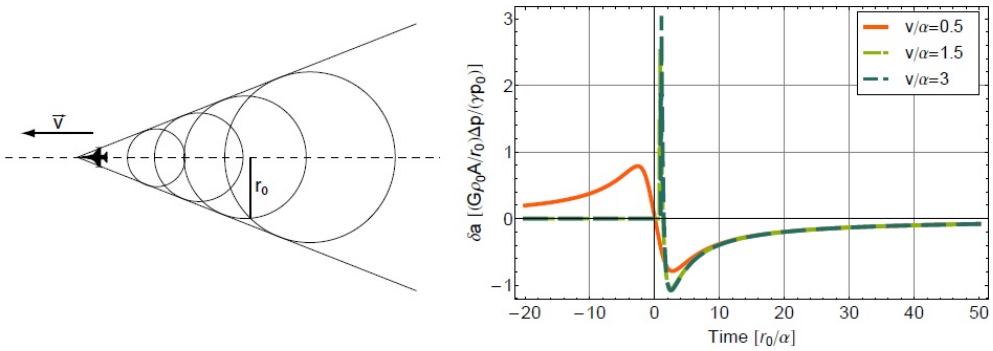

Figure 3: Illustration of the schockwave phenomenon [3].

next generation of laser interferometers (Einstein Telescope, Cosmic Explorer) and for ground-based sub-Hertz detectors.

3 Infrasound NN model

We consider a simple model with a sound wave described as a plane wave of amplitude $\delta p(\omega)$, incident to the surface of the Earth, and reflected without losses [5]. Combining equations 2.1 and 2.2, we can write the associated perturbation of the gravity field. In cylindrical coordinates and integrating over the half-space H for $z > 0$, we find :

$$\delta\Phi(\vec{r_0}, t) = -\frac{G\rho_0}{\gamma p_0} e^{i(\vec{k_\rho}.\vec{\rho_0} - \omega t)} \delta p(\omega) \int_H dV \frac{(e^{ik_z z} + e^{-ik_z z}) e^{i\vec{k_\rho}.\vec{\rho}}}{(\rho^2 + (z - z_0)^2)^{1/2}} \tag{3.1}$$

with $\vec{\rho}$ the radial coordinate, z the vertical coordinate, $\vec{k_\rho}$ the horizontal component of the wave vector, k_z the vertical component of the wave vector, $\vec{\rho_0}$ and z_0 the cylindrical coordinates of the point $\vec{r_0}$.

The direct calculation of this integral gives :

$$\delta\Phi(\vec{r_0}, t) = 4\pi \frac{G\rho_0}{\gamma p_0} e^{i(\vec{k_\rho}.\rho_0 - \omega t)} (e^{-k_\rho |z_0|}(2\Theta(z_0) - 1) - 2cos(k_z z_0)\Theta(z_0)) \frac{\delta p(\omega)}{k^2} \tag{3.2}$$

where $\Theta(z_0)$ is the Heaviside function.

Using the expression of the gravitational potential in equation 3.2, we can find the gravitational acceleration induced by taking the derivative with respect to the direction of interest (for example along the x axis of an arm of the interferometer). Now that we know the acceleration $g(t)$ felt by the test masses and considering the arm's length L, we can write Newton's second law for the strain $h(t) = \Delta L/L$ felt by the interferometer :

$$\ddot{h}(t) = g(t)/L \tag{3.3}$$

Thus, we have all the tools we need to calculate the Fourier transform $h(\omega)$ of this expression and the power spectral density using $\pi S_h(\omega)\delta(\omega - \omega') = \langle h(\omega)h^*(\omega')\rangle$ to study the noise in terms of the frequency.

The coherence length of a sound wave field is typically smaller than its wavelength. For waves of 1Hz we will then have a coherence length of about 340m ($c \simeq 340$ m s^{-1}). In view of the fact that our interferometer has

arms of 3km, the noises felt by each mirror will be completely uncorrelated from one another. This way, to find the total infrasound noise seen by the interferometer, we just have to take the incoherent sum of the noises felt by each arm.

In integral 3.1, we have considered an open half-space for $z > 0$. In reality, as the mirrors are placed in vacuum chambers, inside a building, we need to separate the integral in two contributions : one "exterior" and one "interior" (to which we subtract the part under vacuum containing the detector test masses, as sound waves can't propagate there).

We see in figure 4 an estimate of the AdV infrasound NN which also take into account a model for the test mass buildings [5].

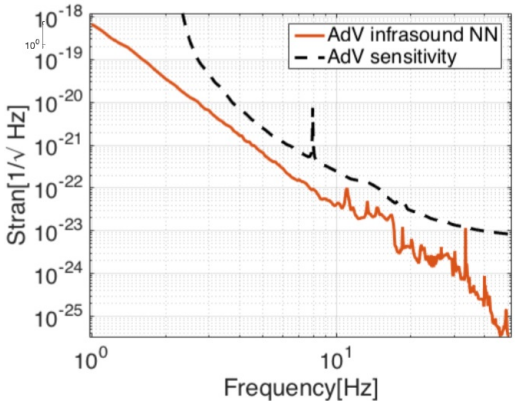

Figure 4: Limit of Virgo sensitivity against infrasound NN estimate.

It is also important to notice that as the mirrors are inside buildings, it is highly probable that the acoustics of the room has a strong influence on the distribution in frequency of the noise. At resonant frequencies, the normal modes associated to the building would produce compression and depression zones of air that can affect the estimate of infrasound NN. This can manifest itself as differences in sound spectra at different positions inside the buildings and in correlation losses between sounds measured simultaneously at different locations because of the inhomogeneity of the pressure field at certain frequencies. The aim of the present work is to highlight the mentioned effects.

4 Room acoustics

Room acoustics is the study of the propagation of sound inside a building according to its geometrical and physical properties. We distinguish two cases [7]:

- **Modal case** : For wavelength in the order of the building's dimensions, the normal modes will be excited for their associated resonant frequencies.
- **Diffuse case** : For wavelength much shorter than building's dimensions, the sound field will be diffuse and homogeneous inside the whole volume.

We define the *Schroeder frequency* as the limit frequency for which we are in one case or the other [6]. We will see its expression later.

4.1 Reverberation time

In diffuse field, we have what we call the reverberation phenomenon. It is the persistence of the sound in the room after interruption of the source until attenuation. It finds its origin in the multiple reflections on the walls. The reverberation time $RT60$ is defined as the time needed for the source to be attenuated by 60dB after interruption [7].

Let's make a simple model for a building in 1 dimension of length L [7]. A wave is emitted incident to the wall with an initial amplitude A_0. After the first reflection, a fraction of the wave is transmitted (absorbed by the wall). The amplitude of the wave reflected one time is then :

$$A_1 = RA_0 = (1-T)A_0 \tag{4.1}$$

with R the reflection coefficient and T the transmission coefficient, the energy conservation gives $R+T=1$. Because of that, we have R et $T<1$.

For the n-th reflection we can write for the amplitude of the wave :

$$A_n = R^n A_0 = (1-T)^n A_0 \tag{4.2}$$

For a speed of sound c_s, it takes a time $\Delta t = L/c_s$ to cross a room of length L. In the continuous limit, for an elapsed time t after its emission, we can say that the wave is at its n-th reflection with $n \simeq t/\Delta t = c_s t/L$, which allows us to write A_n :

$$A(t) = A_0(1-T)^{c_s t/L} = \boxed{A_0 \ \exp\left(\frac{c_s t}{L} ln(1-T)\right)} \tag{4.3}$$

As $0<T<1$, $ln(1-T)<0$. We have an exponential decay profile depending on the size of the room and the absorption of the walls. The larger the room and the weaker the absorption of the walls (strong reflection), the longer the reverberation time will be. When the length L to travel between two reflections is huge, the continuous limit is no longer valid and we don't have reverberation anymore but echo.

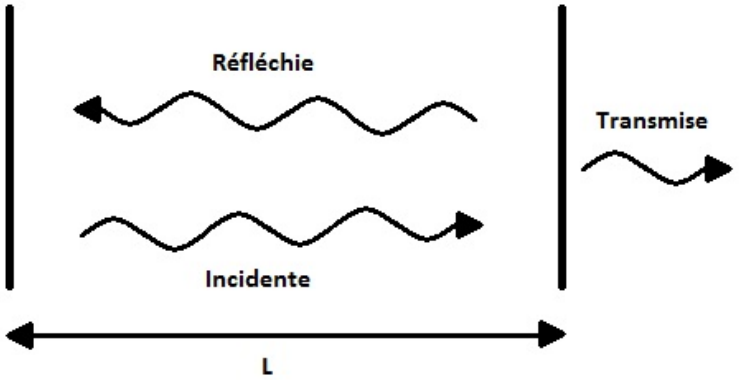

Figure 5: Reverberation inside a room of length L.

The knowledge of the reverberation time $RT60$ allows us to calculate the Schroeder frequency defined as :

$$f_s = 2000\sqrt{\frac{RT60}{V}} \tag{4.4}$$

with V the volume of the building.

4.2 Normal modes in room acoustics

4.2.1 Theory

At low frequencies, successive reflections of the waves lead to stationary modes built by constructive interference for wavelength multiple of the building's dimensions. Such stationary waves obey the Helmholtz equation [8] :

$$(\vec{\nabla}^2 + \vec{k}^2)P(\vec{r}) = 0 \tag{4.5}$$

with $\vec{\nabla}$ the nabla operator, $\vec{k}$ the wave vector and $P(\vec{r})$ the pressure field.

This equation has many solutions depending on the geometry of the system. The simplest case is the parallelepiped in Cartesian coordinates. The 3 contributions in x, y, z of the wave function decouple so we can proceed with a variable separation. It allows us to write :

$$P(x, y, z) = P_x(x)P_y(y)P_z(z) \tag{4.6}$$

Injecting this result in equation 4.5 and writing the norm of the wave vector in Cartesian coordinates, we have :

$$\frac{1}{P_x(x)}\frac{\partial^2}{\partial x^2}P_x(x) + \frac{1}{P_y(y)}\frac{\partial^2}{\partial y^2}P_y(y) + \frac{1}{P_z(z)}\frac{\partial^2}{\partial z^2}P_z(z) + k_x^2 + k_y^2 + k_z^2 = 0 \tag{4.7}$$

We now have 3 independent equations for each direction :

$$\partial_i^2 P(x^i) + k_i^2 P(x^i) = 0 \tag{4.8}$$

with $i = 1, 2, 3 \leftrightarrow x$, y, z.

Using Neumann boundary condition, the normal speed cancels at the walls. That is to say that our walls are infinitely rigid, and their acoustic impedance is infinite. Therefore, using the conservation of momentum for a perfect fluid :

$$\vec{\nabla}P = -\rho_0 \frac{\partial \vec{v}}{\partial t} \tag{4.9}$$

and for a room of length L_x along x, we have :

$$\frac{\partial P_x}{\partial x}(x = 0 \ ou \ L_x) = 0 \tag{4.10}$$

Taking into account the boundary conditions, we find for the general solution along x :

$$P_x(x) = A\cos(k_x x) \tag{4.11}$$

with

$$k_x = \frac{n_x \pi}{L_x} \tag{4.12}$$

where n_x is an integer.

By applying the same procedure for P_y and P_z, and taking into account the expression of P in equation 4.6, we write :

$$P(x,y,z) = P_0 \ \cos(\frac{n_x\pi}{L_x}x)\cos(\frac{n_y\pi}{L_y}y)\cos(\frac{n_z\pi}{L_z}z) \tag{4.13}$$

We can now write the total wave number :

$$k = \pi\sqrt{\left(\frac{n_x}{L_x}\right)^2 + \left(\frac{n_y}{L_y}\right)^2 + \left(\frac{n_z}{L_z}\right)^2} \tag{4.14}$$

For a plane wave, we have $\omega = kc_s = 2\pi f$ so the resonant frequencies are :

$$f = \frac{c_s}{2}\sqrt{\left(\frac{n_x}{L_x}\right)^2 + \left(\frac{n_y}{L_y}\right)^2 + \left(\frac{n_z}{L_z}\right)^2} \tag{4.15}$$

with c_s the speed of sound.

The functions $P(x,y,z)$ define the basis of solutions for each triplet $(n_x,\ n_y,\ n_z)$. Any linear combination of these functions will be solution of the equation 4.5.

We observe 3 types of modes :

- **Longitudinal** : if at least 1 $n_i \neq 0$,
- **Transverse** : if at least 2 $n_i \neq 0$,
- **Oblique** : if the 3 $n_i \neq 0$.

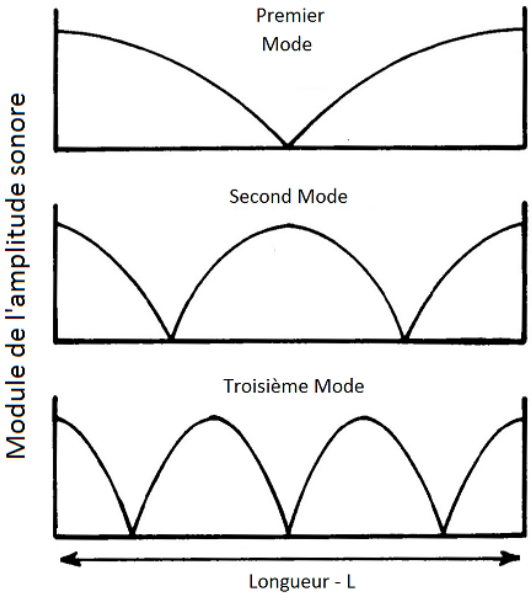

Figure 6: First modes of a building of length L.

In the modal case, we see that the amplitude of the pressure field strongly depends on the position.

4.2.2 North End Building (NEB) simulation

First, we can model the NEB as a parallelepiped of dimension 25×17×17m (L×W×H). Using the equations in last section, we can estimate the resonant frequencies of the building. The tool *amroc* on the website https://amcoustics.com/tools/amroc?l=2500&w=1700&h=1700&r60=4.5 calculates them and "roughly" plots the distribution of the associated modes in the volume. We find :

1	6.86 Hz	A-2	1-0-0	ax
2	10.09 Hz	E-1	0-0-1	ax
3	10.09 Hz	E-1	0-1-0	ax
4	12.2 Hz	G-1	1-0-1	tan
5	12.2 Hz	G-1	1-1-0	tan
6	13.72 Hz	A-1	2-0-0	ax
7	14.27 Hz	A-1#	0-1-1	tan
8	15.83 Hz	B-1	1-1-1	obl
9	17.03 Hz	C0#	2-0-1	tan
10	17.03 Hz	C0#	2-1-0	tan

Figure 7: 10 first possible modes of the NEB (amroc).

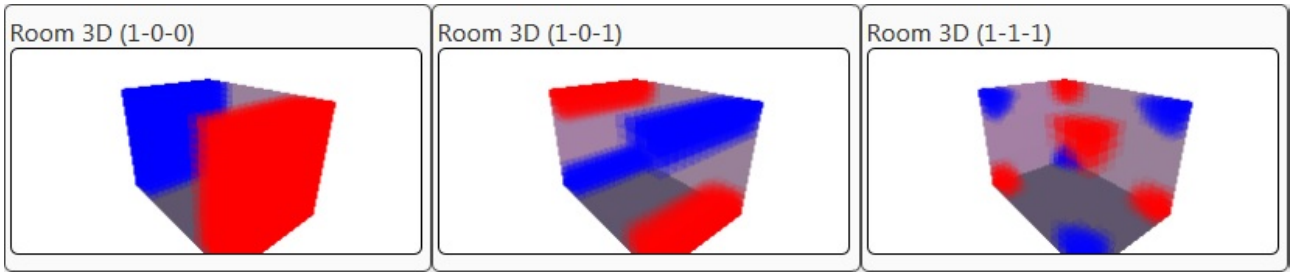

Figure 8: 3D distribution of modes 1, 4 and 8 (amroc), the red and blue zones represent the pressure maximums.

It gives us an idea of the range in which we should find these resonant frequencies. Moreover, we have degeneracy of modes in frequency. It comes from the fact that we have same height and width for our building (17m for both). However, by looking at figure 19 in appendix or figure 9, we clearly see that the NEB's geometry is far more complicated. A more thorough study would need an exact 3D model of the building using simulation softwares.

We launch another simulation using the software COMSOL. We use the same dimensions as previously, adding the vacuum cylinder with the square structure that faces it. We see in figure 9 that it has a significant influence on the distribution of modes, especially that the degeneracy disappears. It also modifies the resonant frequencies.

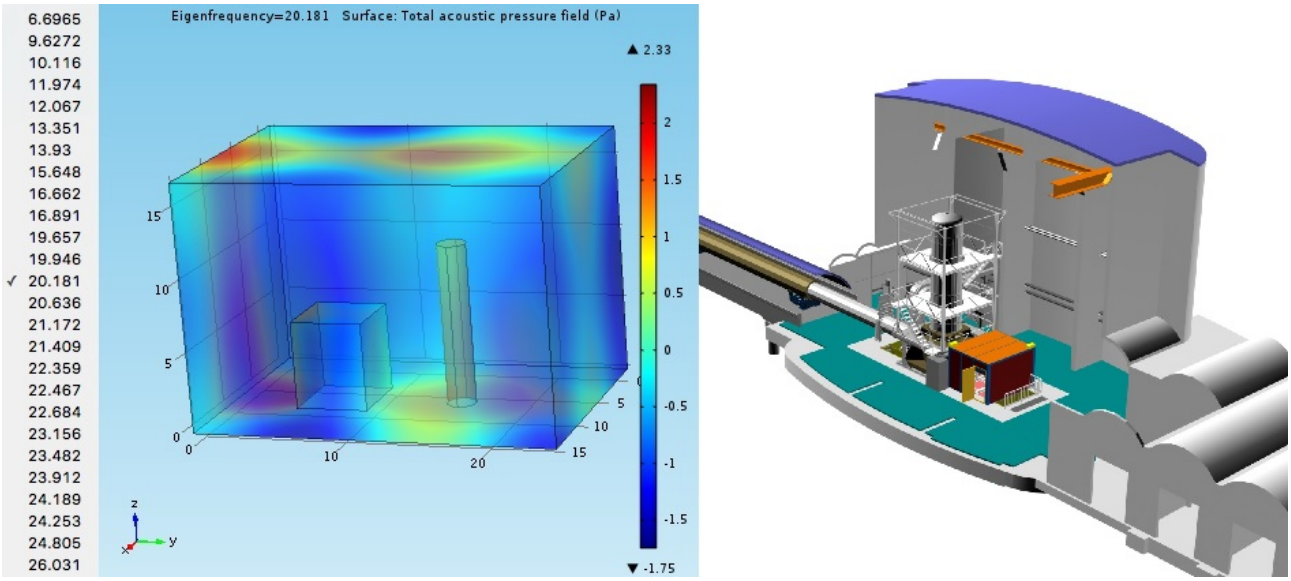

Figure 9: Simple model of the NEB used on COMSOL (with resonant frequencies on the left) VS exact model (right).

We expect to see resonance from 6 Hz. In theory, the number of modes increases with frequency. It means that the higher the frequency, the closer the modes are distributed (hard to distinguish).

5 Measurements on Virgo site (18-22/06/2018)

During the week from June 18th to 22th, we went on the VIRGO site to make the acoustic measurements we needed. They have been made inside the North End Building (NEB), where lies one of two mirrors of the interferometer.

5.1 Measuring principle

We use infrasound microphones Brüel & Kjær microphones, model 4193-L-004 [9], that have a flat response down to 0.5 Hz, connected to amplifiers NEXUS 2690 operating on a bandwidth from 0.1Hz to 100kHz.

As we have seen in the previous sections, the measurement of the infrasound field allows us to estimate the fluctuations of the gravity field. In our case, we will focus our work on the normal modes of the building.

To highlight the effect of the normal modes of the room, we make correlation measurements. Two microphones A and B are used simultaneously. We place them at different points of the building, keeping them separated by 3 or 5m. Once the acquisition has started, we have to leave the building to avoid any additional noise we could be responsible for. We leave it run for 20 min to increase the precision.

The normal modes, in contrast with the diffuse field, produce inhomogeneously distributed sound inside the room. Thereby, two microphones at two different positions might see two different signals at resonant frequencies. This should manifest itself as a correlation loss (hole) between the two microphones for these particular frequencies.

5.2 Reverberation

The first step of the work is to evaluate the Schroeder frequency. To do so, we need to know the reverberation time $RT60$ of the room.

We use impulsional sources like balloons and firecrackers. We then have to study the evolution of the sound pressure level in logarithmic scale (dB) defined as :

$$Sound\ Pressure\ Level = 10 \log \left\{ \left(\frac{P_{eff}}{P_{ref}} \right)^2 \right\} \tag{5.1}$$

with P_{eff} the RMS pressure measured in Pascal and P_{ref} a reference pressure in Pascal.

The amplitude's decay being exponential because of the reverberation, we expect to have a linear decay in logarithmic scale. The $RT60$ represents the time it takes for the signal to decrease by 60dB after its interruption at t_0 :

$$Sound\ Pressure\ Level(RT60) \ - \ Sound\ Pressure\ Level(t_0) = -60 \tag{5.2}$$

In general, the precision of the measurement is limited by the background noise. To perform a direct calculation of $RT60$, one needs a source that is powerful enough to exceed the background noise by 60dB, which is very hard to execute. Instead, we estimate the $RT20$ or the $RT30$ which are simply the time it takes for the signal

to respectively decrease by 20 and 30dB. Given the linear behaviour of the decay, knowing the $RT20$ or the $RT30$, we can extrapolate $RT60$ by taking [10]:

$$RT60 = 2 \times RT30 = 3 \times RT20 \tag{5.3}$$

The protocol to estimate the reverberation time is the following [10]:

After importing the whole signal the first thing to do is slicing it from the explosion. Then, one proceeds to a RMS envelope fit to get the exponential behaviour. From this fit, one then calculates the sound pressure level (dB). The valuable part of the signal is to be taken around -5dB after the boom and +10dB above background noise level. After estimating the mean background noise level from a sample taken 5s before explosion, proceed to a linear fit in the dB region previously mentioned. This fit allows us to determine $RT20$ and extrapolate $RT60$.

On plot 11, the red dotted line is the mean background noise level, the blue lines delimit the region of interest.

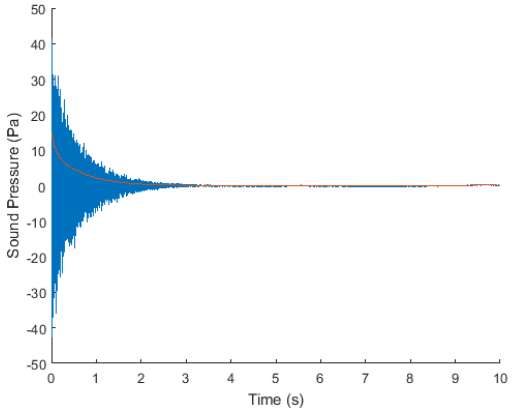

Figure 10: Raw signal of the explosion with RMS envelope fit.

In total, we blew up 2 balloons and 2 firecrackers and each explosion was recorded simultaneously with 2 microphones (A and B) placed at the two extremities of the NEB. It seems that the balloons we used were too weak compared to the background noise. Only the signals we had using firecrackers were good enough to measure the $RT20$.

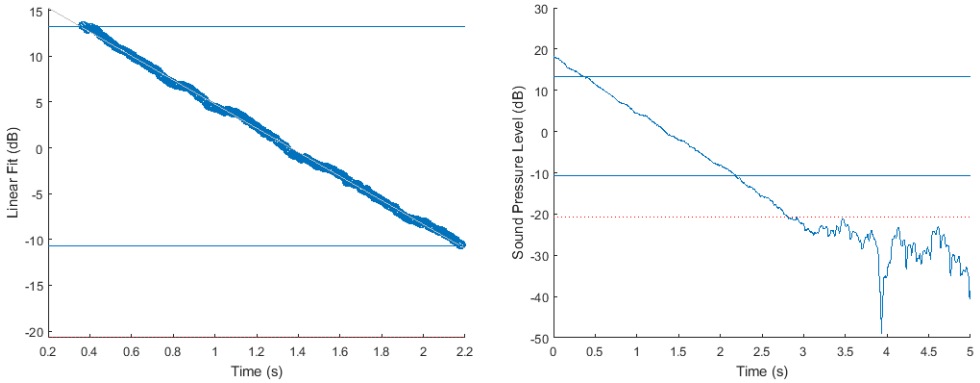

Figure 11: Linear fit of signal's decay for $RT20$ estimate.

We gather the results in these tables :

	$RT20$ (s)	$RT60$ (s)
Micro A	1.46	4.38
Micro B	1.53	4.59

Table 1: Reverberation time for firecracker n°1

	$RT20$ (s)	$RT60$ (s)
Micro A	1.48	4.43
Micro B	1.53	4.58

Table 2: Reverberation time for firecracker n° 2

Hence, we have for the mean $RT60$:

$$\boxed{RT60 = 4.5 \pm 0.2s} \tag{5.4}$$

Finally, we can estimate the Schroeder frequency, considering the NEB a rectangular volume of dimensions $25 \times 17 \times 17$ m $= 7225m^3$. We find :

$$f_s = 2000\sqrt{\frac{RT60}{V}} \simeq 50 \text{ Hz} \tag{5.5}$$

It means that for frequencies under 50 Hz, we are exciting the normal modes of the room.

The reverberation time depends on the frequency. By treating the signal with an octave band filter we can show its dependence on frequency. We use the bands 125, 250, 500, 1000, 2000, 4000 et 8000Hz. The result is plotted on figure 12.

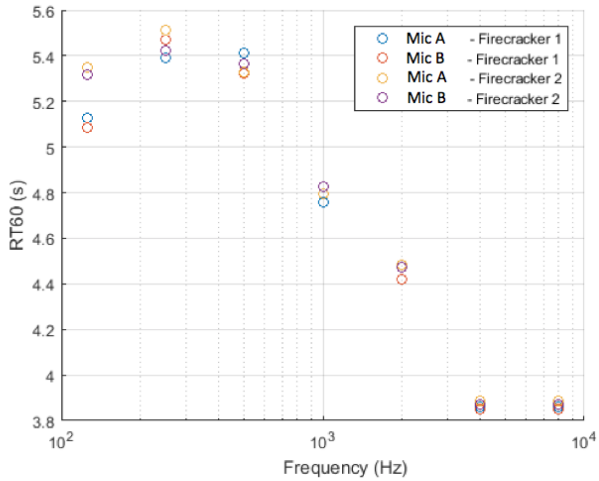

RT60(s)		125 Hz	250 Hz	500 Hz	1000 Hz	2000 Hz	4000 Hz	8000 Hz
Firecracker 1	MicA	5.1290	5.3936	5.4100	4.7556	4.4855	3.8582	3.8582
	MicB	5.0876	5.4713	5.3246	4.7940	4.4190	3.8506	3.8506
Firecracker 2	MicA	5.3489	5.5116	5.3302	4.7965	4.4838	3.8893	3.8893
	MicB	5.3189	5.4229	5.3636	4.8283	4.4719	3.8693	3.8693

Figure 12: $RT60$ as a function of frequency (mic EGO = mic A, mic APC = mic B).

On average we find ∼4.7 sec. We see that the maximum value lies in the low-medium frequency range (250Hz). When we get closer to 50Hz, the reverberation times calculated make no more sense [7]. We observe gaps of 4s between the $RT60$ measured by one microphone and the other. Indeed, as we are near the Schroeder frequency, we switch to the modal case and the reverberation time strongly depends on frequency and position. Therefore, these values are excluded.

5.3 Correlations

To study the correlation inside the volume of the building, we separate our two microphones by a distance of about 3m, horizontally or vertically. This way we can see the modes in the two directions. We try to take as much points as possible to cover the whole surface of the NEB.

Once the measurements are obtained, we process them with a MATLAB program already used in [5] to calculate the correlation between the two microphones.

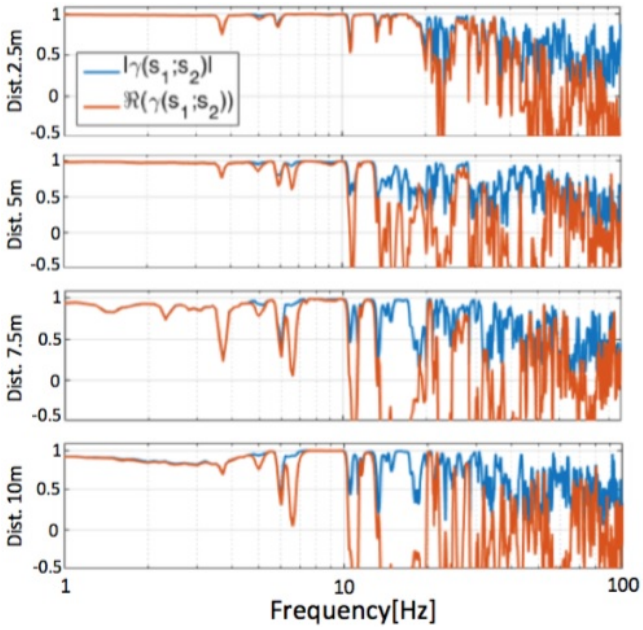

Figure 13: Correlation measurements inside the NEB [5] (in blue : absolute value; in red : real part). We see that the correlation losses intensify as we move the microphones away from one another and for higher frequencies.

5.3.1 Horizontal measurements

In total, we used 16 different positions (see figure 14), each time with two microphones A and B respectively named EGO and APC, both at same height. The measurements 13 and 14 are the same, with the microphones pointing toward the inside for the 13 and toward the outside for the 14, to check if the measurement depends on their orientation (it will eventually show up that it does not, as expected). The correlations for each horizontal measurement are gathered in Figure 20.

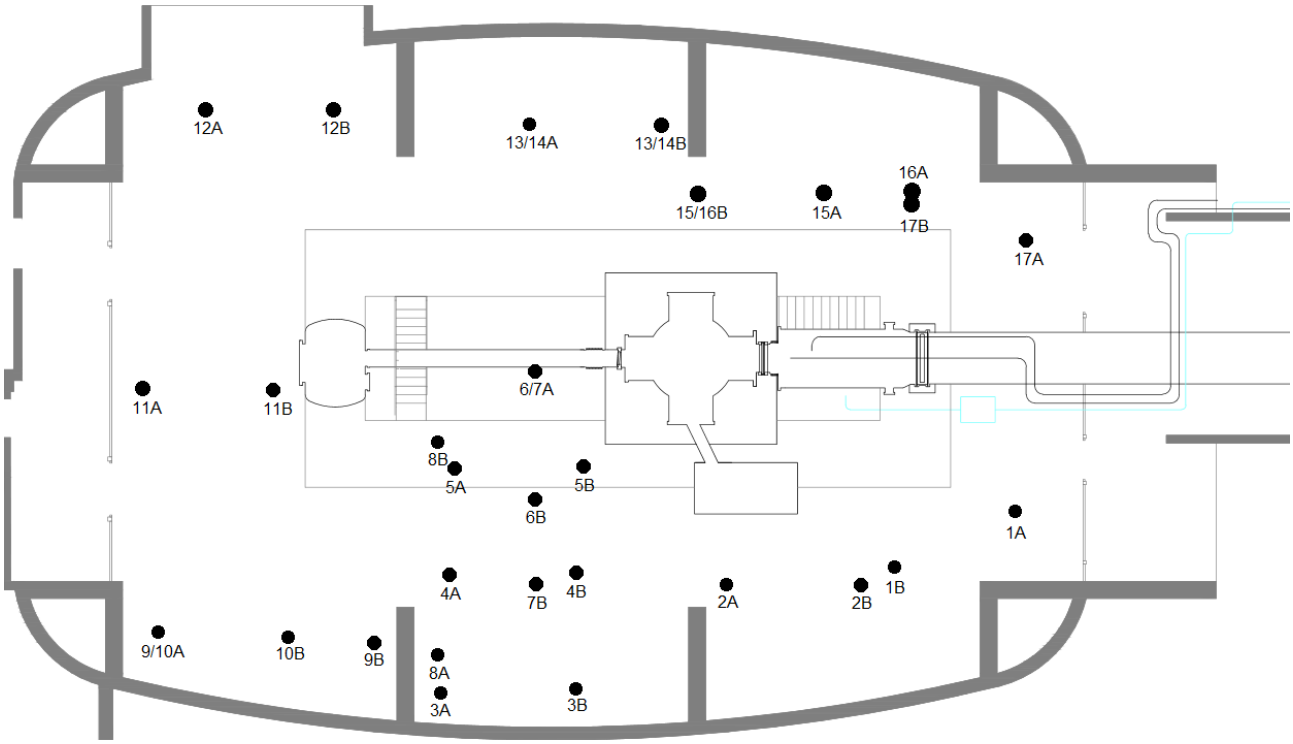

Figure 14: Measurement positions inside the NEB

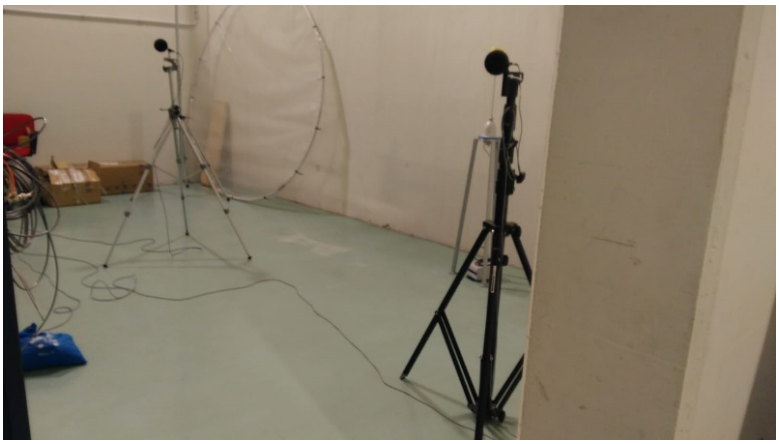

Figure 15: Horizontal measurement 13

5.3.2 Vertical measurements

For vertical measurements, we reuse the previous positions, this time placing both microphones on the same point at different heights. Mic A is placed at 67cm above ground and mic B, having the longest microphone stand, with a maximum height of 455cm, is placed higher (see figure 16).

We perform 13 other measurements, at different positions and heights. The vertical correlations are gathered in Figure 21.

Figure 16: Vertical measurement 19

6 Results

6.1 Horizontal measurements

Given the axial symmetry of the NEB's structure, modes should be distributed symmetrically along the axis of the laser interferometer arm. This implies similarities between measurements from 1 to 11 and measurements from 11 to 17. We indeed observe this symmetry when we look at the frequency spectrum of microphones 1B and 17B individually : they are nearly identical even though they were measured at different time and position. If we compare them with position 13, we see a drastic change of the signal around 6-7Hz, which strongly indicates the presence of the mode (1 0 0), as illustrated on figure 8. The microphones 1 and 17 lie on the pressure maximum, while the 13 lies on the minimum.

According to the simulations we performed in the previous section, we should find correlations losses around 6-7Hz (mode (1 0 0)), and 10Hz (mode (0 1 0)). When looking at figure 20, we do see these holes. However, above 10Hz, the hole distribution becomes extremely complex. To be able to carry out any further studies, we would need a precise 3D model of the NEB to accurately simulate its acoustics using COMSOL. This work is currently in progress.

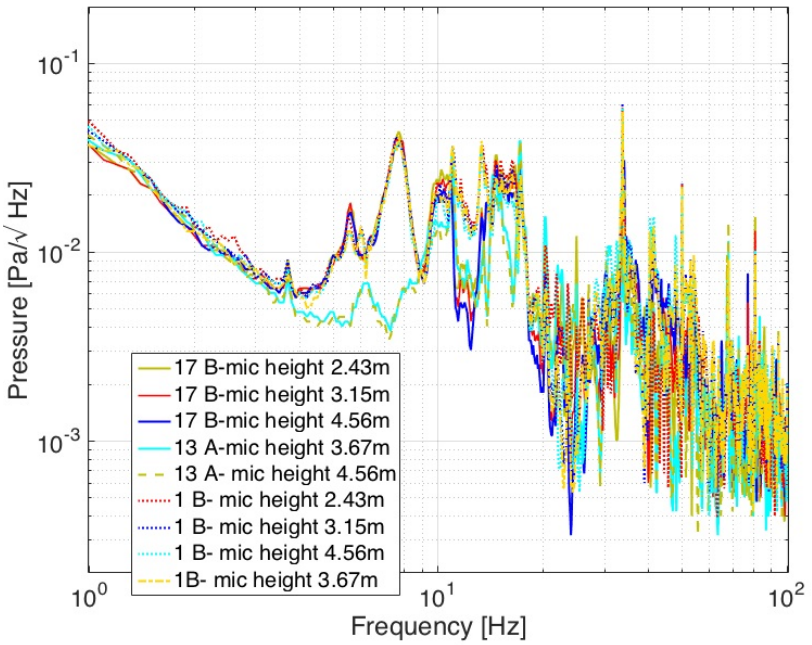

Figure 17: Comparison of different signals at different positions.

A hole is always present at 4Hz. Yet, it seems that this hole is not connected to a mode but to a microphone defect. If we look at the frequency spectrum of microphones A and B, we see that a peak always shows up at 4Hz for mic B while none is observed for mic A. Because of this, a hole always appears at 4Hz whenever we calculate the correlations. We shall not take it into account.

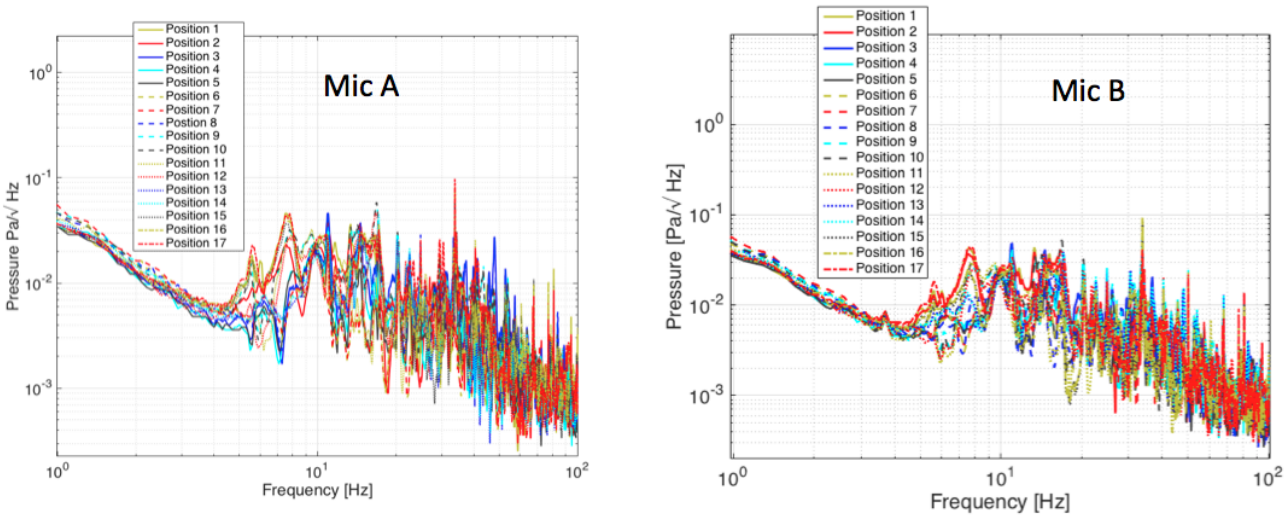

Figure 18: Microphone B defect at 4Hz

At the current analysis stage, we can only say that we do find the correlation losses announced by the simulation at ∼6 Hz and ∼10 Hz. An in-depth study of resonant frequencies above 10Hz requires a new simulation, way more accurate than the previous one.

6.2 Vertical measurements

The mode's distribution for vertical correlations seems less dense than horizontal correlations for frequencies under 10Hz. Again, we find the defect at 4Hz and the pattern gets more complex after 10Hz. For the rest, we get back to the same problem : we are unable to pursue our line of inquiry any further without the exact 3D model.

The lack of modes observed can also come from the fact that we could not cover a broad range of heights with our microphone stand. Indeed, the building is 17m high and the maximum height of our pole is 4.55m.

7 Conclusion

The study of the NEB's acoustics turns out to be a very complicated task. According to the Schroeder frequency, we see that the modal case starts to dominate at frequencies under 50Hz. Yet, we already have a substantial amount of modes above 10Hz that reveals a complex pattern of distributions.

Further studies will consist in a precise simulation of the NEB in order to understand the relation between the distribution of modes and the correlation spectrum we observe. The ultimate goal is the reduction of the detector building acoustic mode impact on the infrasound Newtonian Noise.

8 Appendix

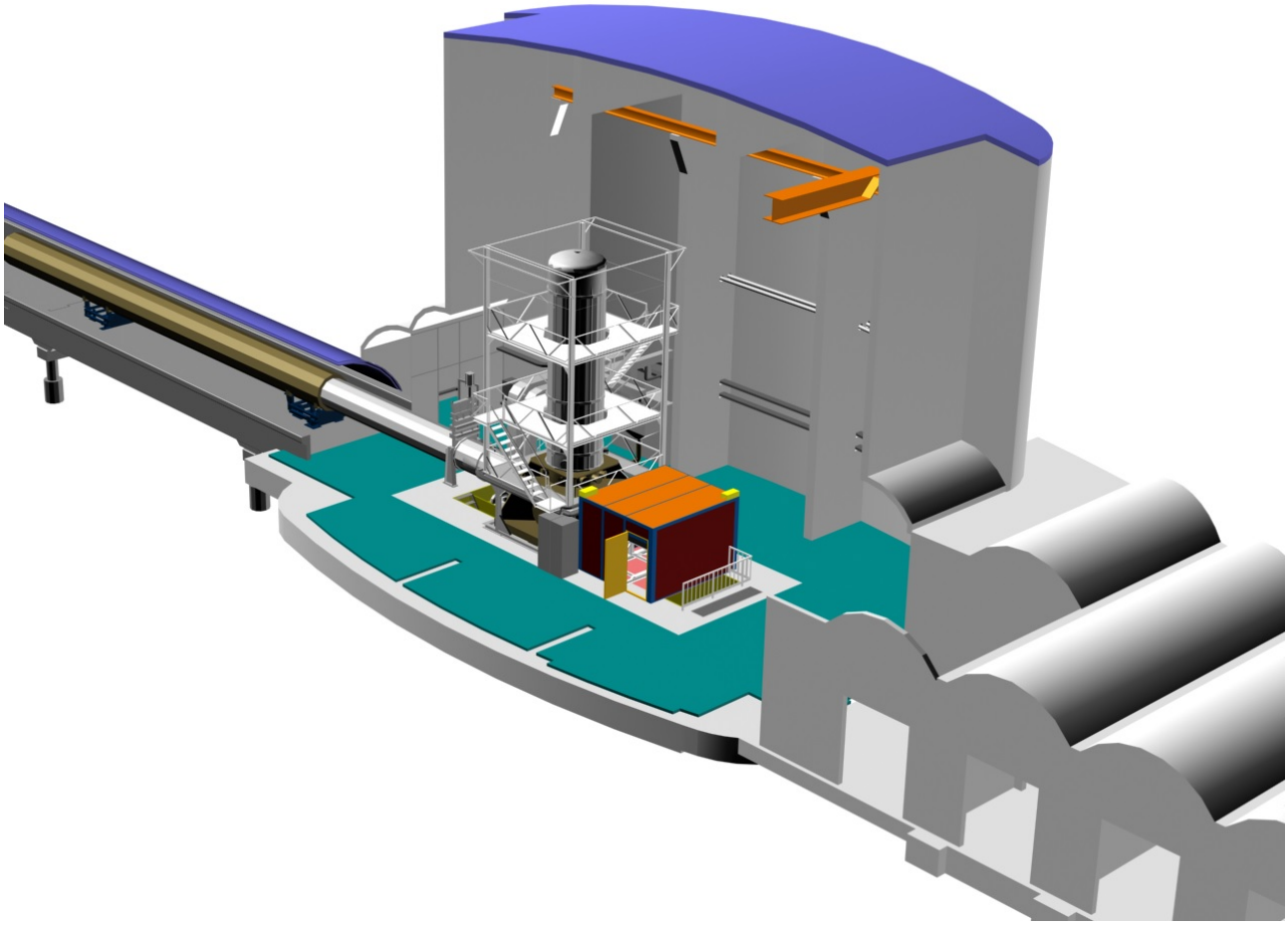

Figure 19: Inside of North End Building. The entrance is on the right, the laser comes from the left. The cylinder in the middle is the vacuum chamber that contains the suspended mirror.

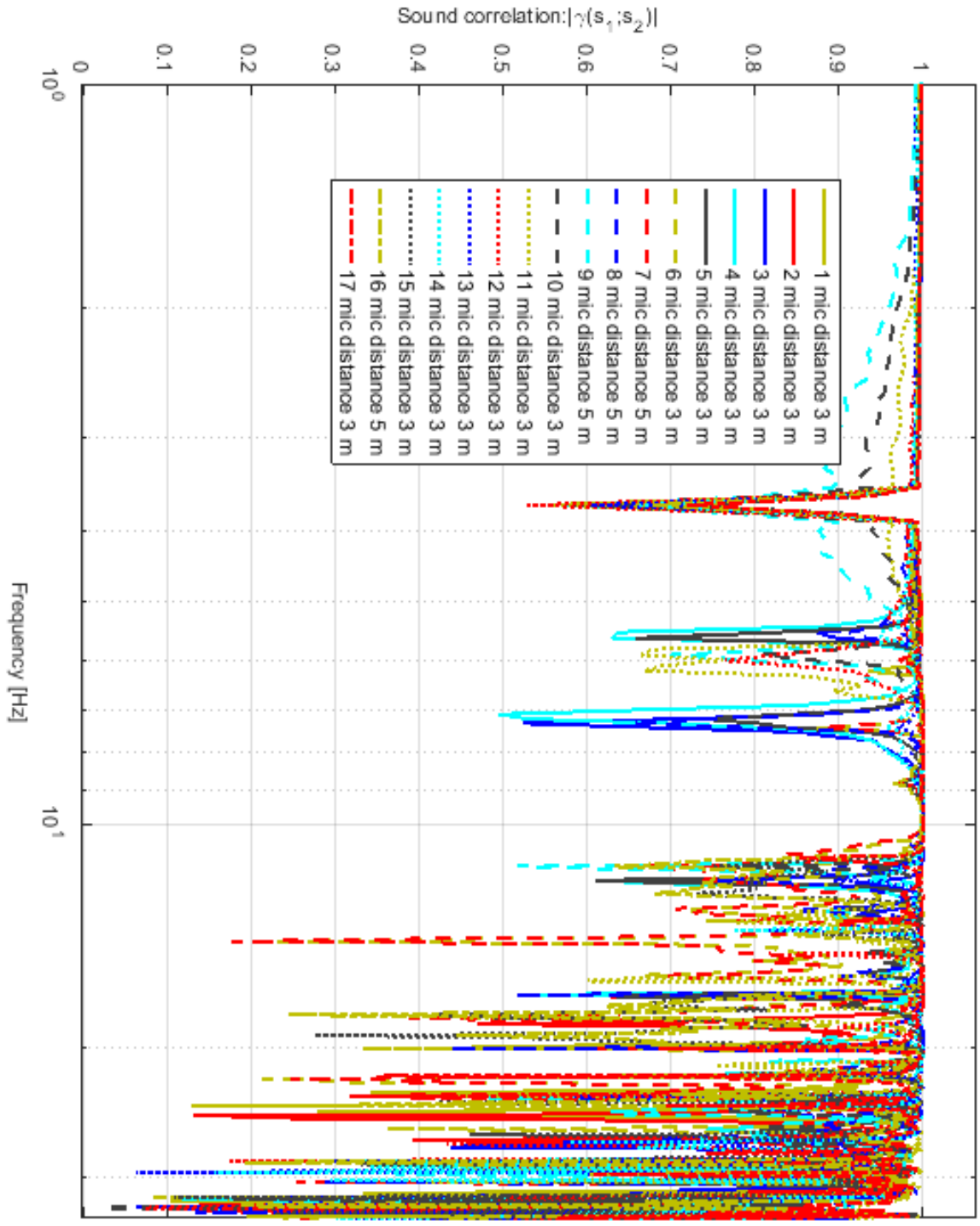

Figure 20: Correlation measurements when moving the microphones horizontally.

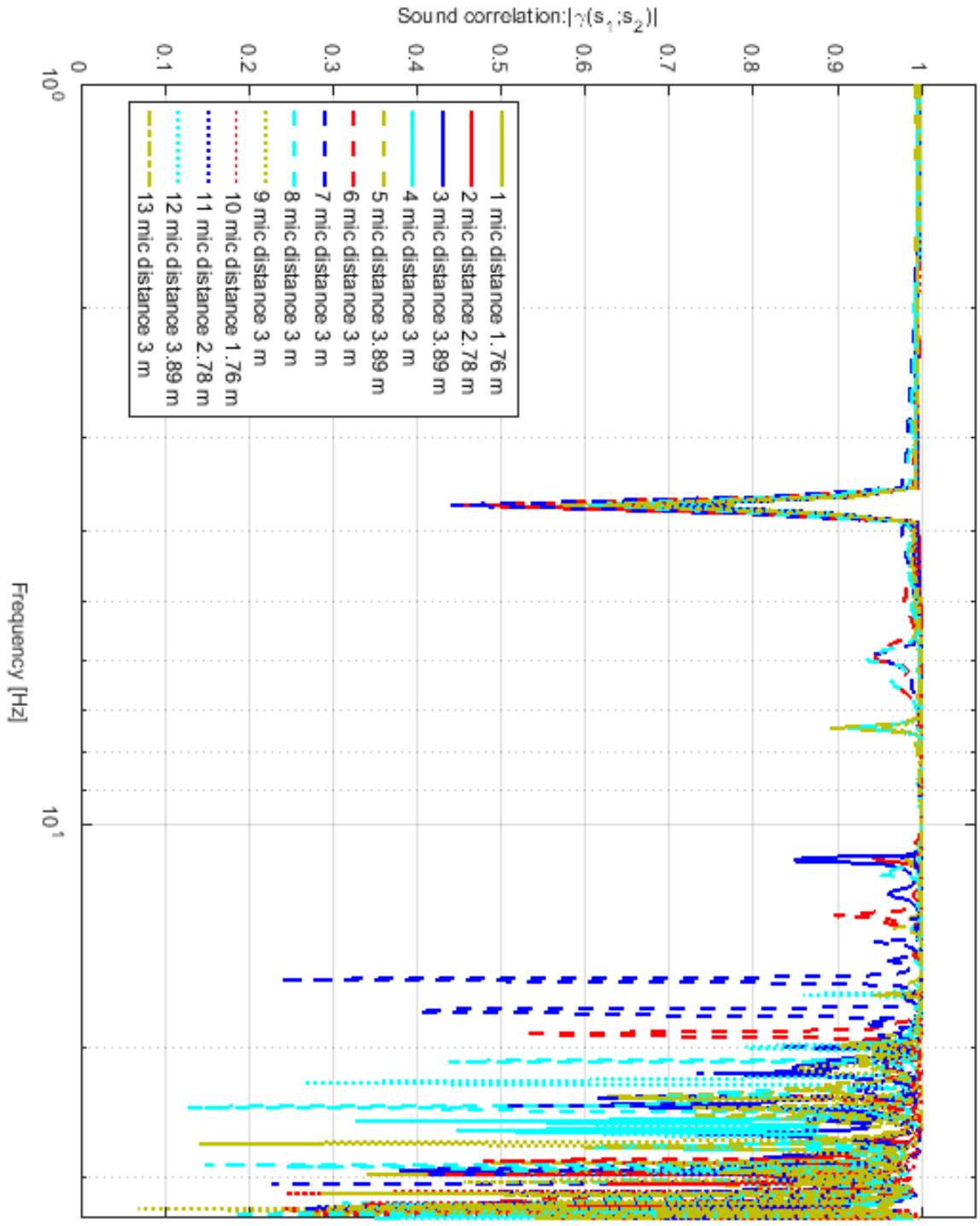

Figure 21: Correlation measurements when moving the microphones vertically.

References

[1] Jan Harms et al., *Low-frequency terrestrial gravitational-wave detectors.* Phys. Rev. D 88, 122003 ? Published 13 December 2013 2

[2] T Accadia et al, *Virgo: a laser interferometer to detect gravitational waves.* 2012 JINST 7 P03012 - DOI 10.1088/1748-0221/7/03/P03012

[3] Jan Harms, *Terrestrial Gravity Fluctuations.* Living Rev. Relativity, 18, (2015), 3 - DOI 10.1007/lrr-2015-3 3, 5

[4] Michele Maggiore, *Gravitational Waves*, Volume 1 3

[5] Donatella Fiorucci, *Impact of infrasound atmospheric noise on gravity detectors used for astrophysical and geophysical applications.* Physical Review D 97, 062003 (2018) - DOI 10.1103/PhysRevD.97.062003 5, 6, 15

[6] Manfred R. Schroeder, *The "Schroeder Frequency" revisited.* The Journal of the Acoustical Society of America 99, 3240 (1996) - DOI: 10.1121/1.414868 6

[7] Université de Nice `http://physique.unice.fr/sem6/2012-2013/PagesWeb/PT/Reverberation/page1.html` 6, 7, 15

[8] Alexandre Leblanc, *Modélisation numérique des résonances par une formulation intégrale - Application au confort acoustique dans une cavité 3D. .* Acoustique [physics.class-ph]. Université d'Artois, 2004. Français. tel-00261712 8

[9] Brüel & Kjær microphone model 4193-L-004, `https://www.bksv.com/en/products/transducers/acoustic/ microphones/microphone-preamplifier-combinations/4193-L-004` 12

[10] Noise Meter Inc. `https://www.noisemeters.com/help/faq/reverb-time.asp`

13